J Mater Sci (2013) 48:6558–6566
DOI 10.1007/s10853-013-7452-0

Inertial stabilization of flexible polymer micro-lattice materials

Sha Yin · Alan J. Jacobsen · Linzhi Wu · Steven R. Nutt

Received: 14 April 2013 / Accepted: 16 May 2013 / Published online: 25 May 2013

Abstract Soft micro-lattice materials with different lattice geometries were fabricated using a self-propagating photopolymer waveguide process. The parent polymer was characterized by dynamic mechanical analysis and the glass transition temperature shifted with equivalent strain rate. Quasi-static and dynamic compression tests were subsequently carried out to investigate the inertial stabilization of lattice member buckling as a function of strain rate and structural geometry (e.g. relative density and lattice aspect ratio). A high-speed digital camera was used to record the progression of deformation and failure events during compression. The micro-lattice structures exhibited super compressibility and increased strength. The observed strength increase, particularly for high aspect ratio and high strain rate, was attributed to inertial stabilization.

Introduction

Lattice materials are ordered cellular structures with efficient, stretch-dominated topology that are well suited for multifunctional applications [1]. These materials have been produced from metals, polymers, and fiber composites using different manufacturing approaches to achieve feature sizes ranging from nanometers to millimeters. For metallic lattice materials, fabrication techniques include investment casting [2, 3], deformation forming [4–7] and metal wire approaches, as reviewed by Wadley [8–10] involved with several applications [11, 12]. Bouwhuis et al. [13] have studied the edge effects of metallic lattice materials in compression. Fiber-reinforced lattice materials fabricated by molding techniques take advantages of the intrinsic properties of fiber composites and outperform metallic counterparts from the standpoint of specific strength and modulus [14, 15]. While metallic and composite lattice materials typically have feature sizes on the order of millimeters, three-dimensional nano-scale lattice structures can be fabricated by photolithographic methods, such as four-beam/holographic interference lithography [16] or two photon photolithography [17]. Polymer lattice materials recently have been fabricated from interconnected patterns of self-propagating waveguides, which generally have feature sizes that fall between the aforementioned approaches [18–20]. The micro-lattice structures feature perfect nodal connectivity and can have multiple unit cells through the thickness of the material. Jacobsen et al. [19] point out that post curing in an oxidizing environment suppresses the tendency for lattice members to prematurely buckle.

Polymers are generally rate-sensitive [21–23], and thus polymer composites [24] and foams [25] are strongly affected by loading rate. The dynamic compressive response of corrugated carbon-fibre reinforced epoxy sandwich cores has been investigated by Kazemahvazi et al. [26] and strength enhancement is observed as loading rate increases. Hutchinson and colleagues have provided significant insights into the dynamic behavior of cellular structures [27–29] and identified three factors contributing to the dynamic strength enhancement of stainless steel

S. Yin · S. R. Nutt
Department of Chemical Engineering and Materials Science, University of Southern California, Los Angeles, CA, USA

S. Yin (✉) · L. Wu
Center for Composite Materials, Harbin Institute of Technology, Harbin 150080, China
e-mail: yinsha2008@gmail.com

A. J. Jacobsen
HRL Laboratories LLC, Malibu, CA, USA

honeycombs: material rate sensitivity, inertial stabilization of the webs against buckling, and plastic wave propagation (controlled by axial inertial). For low-speed impact, the dynamic strength enhancement is primarily due to the inertial stabilization of webs. Moreover, results suggest the majority of the strength enhancement of composite corrugated cores can be attributed to inertial stabilization of the core member [26]. Inertial effects on metallic lattice materials under dynamic loading have been discussed elsewhere [30, 31]. The dynamic compressive behavior of aluminum-alloy-based tetrahedral-core truss structures exhibits inertial stabilization against buckling that depends on loading rates and test temperatures.

The motivation of this work is to investigate the strain-rate sensitivity of polymer micro-lattice structures and the inertial stabilization of lattice member buckling as a function of loading rate and structural features, such as density and lattice geometry. More compliant micro-lattice structures with different geometries were fabricated using techniques described previously [18]. Static and dynamic compression tests were performed to determine the behavior of the parent polymer and the polymer micro-lattice structures. The results allow us to decouple the inertial stabilization contribution due to lattice geometry from the material strain-rate, and the insights provided will guide structural designs to improve crush resistance in engineering applications.

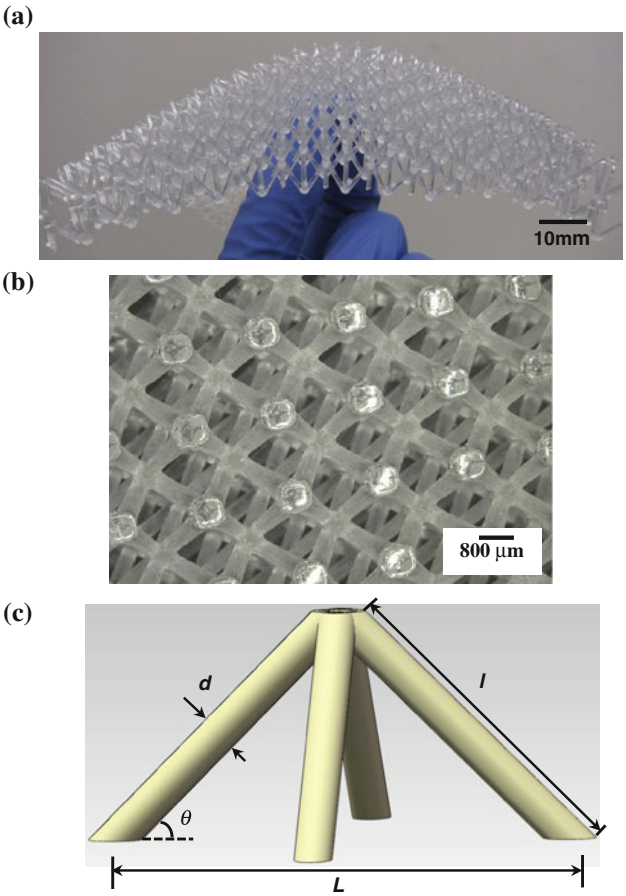

Fig. 1 **a** Flexible polymer micro-lattice structures on fingertips; **b** optical images with repeating octahedral unit cells; **c** sketch of a simple pyramidal configuration (half of the octahedral unit cell) illustrating geometric parameters

Experiments

Polymer micro-lattice fabrication

Flexible polymer micro-lattice structures were fabricated using a self-propagating photopolymer waveguide process developed at HRL Laboratories (Fig. 1). The process involved exposing a mask with a square pattern of circular apertures placed over a liquid thiol-ene monomer system. The mask was exposed simultaneously to four collimated beams generated from a mercury arc lamp. Further details about the process could be found elsewhere [18, 19]. The resulting strut diameter d and length l (Fig. 1c) can be varied by changing the aperture spacing and diameter on the mask, which will result in different d/l. Here, the lattice inclination angle θ was constant at $60 \pm 2^{\circ}$. Seven groups of micro-lattice samples were fabricated with different geometries (see Table 1). Each group consisted of four specimens cut from a single sample of 100×100 mm, and each specimen was bonded to two fiberglass laminates using epoxy adhesive (Hysol EA 9360, Henkel) to form a sandwich structure. All specimens in each group were compressed at four strain rates as described in the following sections.

Dynamic mechanical analysis (DMA)

The glass transition temperature (T_g) of the parent polymer was measured by DMA in dual cantilever mode (DMA: Q800, TA Instruments, Inc., United States). Rectangular specimens were machined ($59.5 \times 12.2 \times 3.5$ mm) and tested between -20 and 80 °C with a heating rate of 3 °C/min. By approximating the applied sinusoidal strain wave with a triangular strain wave, the equivalent average strain rate can be related to dynamic frequency ω as $\dot{\varepsilon} = 2\varepsilon\omega$, where ε was the strain amplitude [22]. Accordingly, we performed tests at frequencies of 1, 10 and 100 Hz with strain amplitude of 0.5 %, which corresponded to strain rates of 0.01, 0.1 and 1/s, expecting a shift in T_g with strain rate.

Quasi-static compression

The quasi-static mechanical behavior (10^{-3}–1/s) of parent polymer rods and polymer micro-lattice sandwich

Table 1 Summary of geometries and properties for polymer micro-lattice structure at different strain rates

Sample	Lattice diameter d (μm)	Lattice length l (μm)	d/l	Density (g/cm^3)	Strain rate (/s)	Peak stress (kPa)
A	840 ± 40	12950 ± 20	(6.50 ± 0.3)E-2	0.044 ± 0.002	0.001	9.85
					0.1	65.58
					50	520.55
					100	2583.69
B	1000 ± 20	11700 ± 20	(8.55 ± 0.18)E-2	0.062 ± 0.002	0.001	13.01
					0.1	138.39
					50	888.28
					100	4154.28
C	780 ± 10	5720 ± 15	(1.36 ± 0.02)E-1	0.079 ± 0.002	0.001	7.06
					0.1	136.97
					50	582.27
					100	1362.77
D	865 ± 28	6020 ± 10	(1.44 ± 0.05)E-1	0.099 ± 0.001	0.001	15.57
					0.1	229.28
					50	1010.82
					100	1184.05
E	480 ± 40	3070 ± 30	(1.56 ± 0.15)E-1	0.144 ± 0.004	0.001	31.11
					0.1	405.7
					50	1419.584
					100	1782.78
F	2530 ± 25	11350 ± 20	(2.23 ± 0.03)E-1	0.220 ± 0.004	0.001	185.93
					0.1	1085.16
					50	2299.75
					100	4657.17
G	1500 ± 50	5790 ± 15	(2.59 ± 0.1)E-1	0.296 ± 0.004	0.001	134.82
					0.1	1469.92
					50	2851.19
					100	5597.87

structures was determined by axial compression tests. The polymer rods were 8 mm in diameter and the micro-lattice sandwich structures were approximately 50 × 50 mm. All tests were conducted using a load frame at strain rates of 0.001 and 0.1/s. The load was measured using a 30 kN built-in load cell with an accuracy of ±1 %, and an external LVDT extensometer mounted on the compression plates was used to control the loading rate and record displacement.

Dynamic compression

High strain rate behavior was investigated using an instrumented drop tower (INSTRON Dynatup 9250HV) equipped with a flat platen. All specimens were placed on a flat circular plate 100 mm in diameter fixed beyond the pneumatic clamping system, which covered the inner ring diameter of 76.2 mm. The mass of the crosshead was maintained at 10.44 kg, and impact velocity was adjusted to achieve the desired strain rate $v = \dot{\varepsilon} \cdot H$, where H is the height of polymer rods or micro-lattice test samples. A data acquisition system recorded load vs. time during impact tests.

A high-speed digital camera with a maximum framing rate of 24000 frames/s was also used to record the deformation history and failure events of the specimens during dynamic compression tests (Keyence VW-6000). The camera was placed near the sample to achieve the required magnification, and configured with an appropriate Hakuba lenses for the best visibility.

Results

Polymer characterization

Dynamic mechanical analysis (DMA)

The storage and loss modulus over a temperature range of −20 and 80 °C are shown in Fig. 2a at frequencies of

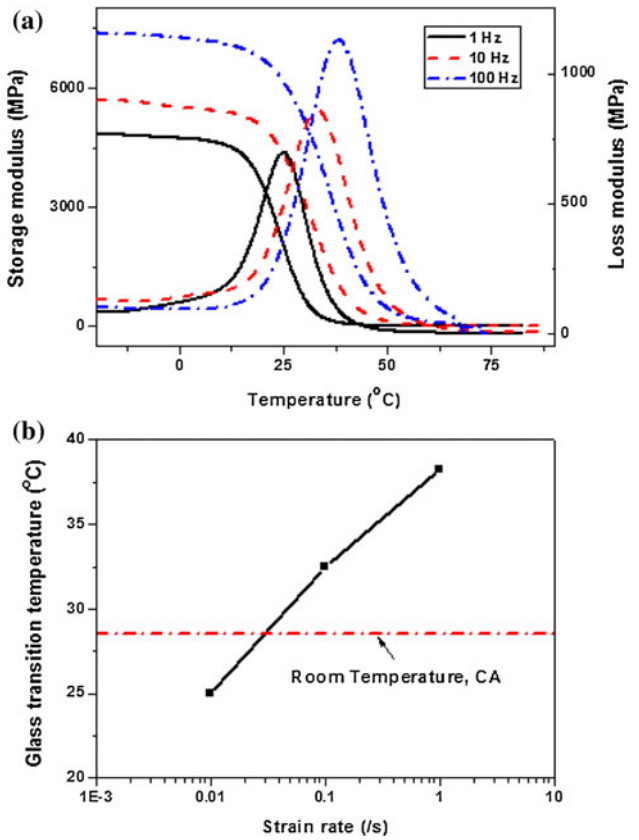

Fig. 2 **a** DMA results of storage modulus and loss modulus as a function of temperature at frequencies of 1, 10 and 100 HZ; **b** shifting of glass transition temperature with strain rates

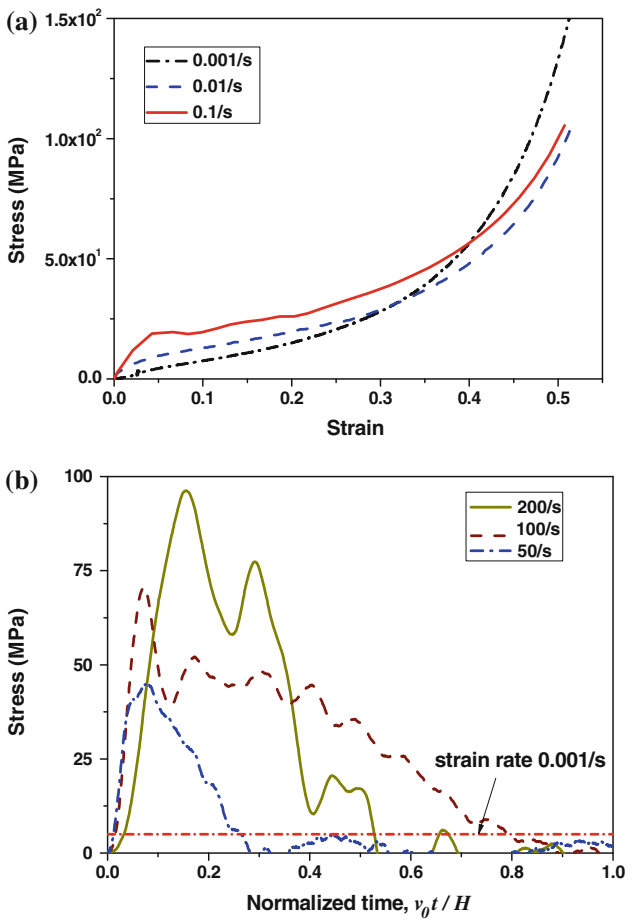

Fig. 3 **a** Compression behavior of parent polymer at strain rates 0.001 and 0.1/s; **b** dynamic stress–time responses at strain rates between 50 and 200/s

1 Hz (0.01/s), 10 Hz (0.1/s) and 100 Hz (1/s), respectively. The glass transition temperature T_g was taken as the peak in the loss modulus, which is related to the physical property changes attributed to the glass transition, and the corresponding dependence on strain rate is plotted in Fig. 2b. The shift rate is about 6.6 °C per decade strain rate. T_g at 1 Hz (0.01/s) is 25 °C, and thus the extrapolated T_g at quasi-static strain rate 0.001/s is 18.4 °C which is below room temperature T_r. Thus, the polymer will be in a rubbery state for $T_g < T_r$, while exhibits glassy state for those with $T_g > T_r$. Accordingly, the polymer micro-lattice structures are flexible, as shown in Fig. 1a.

Strain rate sensitivity of parent polymer

The static compressive response of the parent polymer is shown in Fig. 3a among strain rate range 0.001–0.1/s. The compressive stress–strain curves exhibited an initial stiff behavior, followed by plastic flow of the polymer. Because the polymer did not display an obvious yield behavior, the initial modulus was determined from the stress-strain slope compressed to 2 %, and the strength values at different strain rates were termed as the stress levels at the specific strain 5 %. Additionally, the response of the polymer at strain rates between 50 and 200/s are shown in Fig. 3b, compared with the strength at strain rate of 0.001/s, which is included as a horizontal dashed line. The strength increase with strain rate indicates the rate-dependency of the polymer.

Properties of polymer micro-lattice sandwich structures

Seven groups of micro-lattice sandwich structures with different aspect ratios and densities were tested at different strain rates as summarized in Table 1.

Quasi-static compression behavior

Stress-strain curves in quasi-static compression (0.001 and 0.1/s) are shown in Fig. 4a for three representative

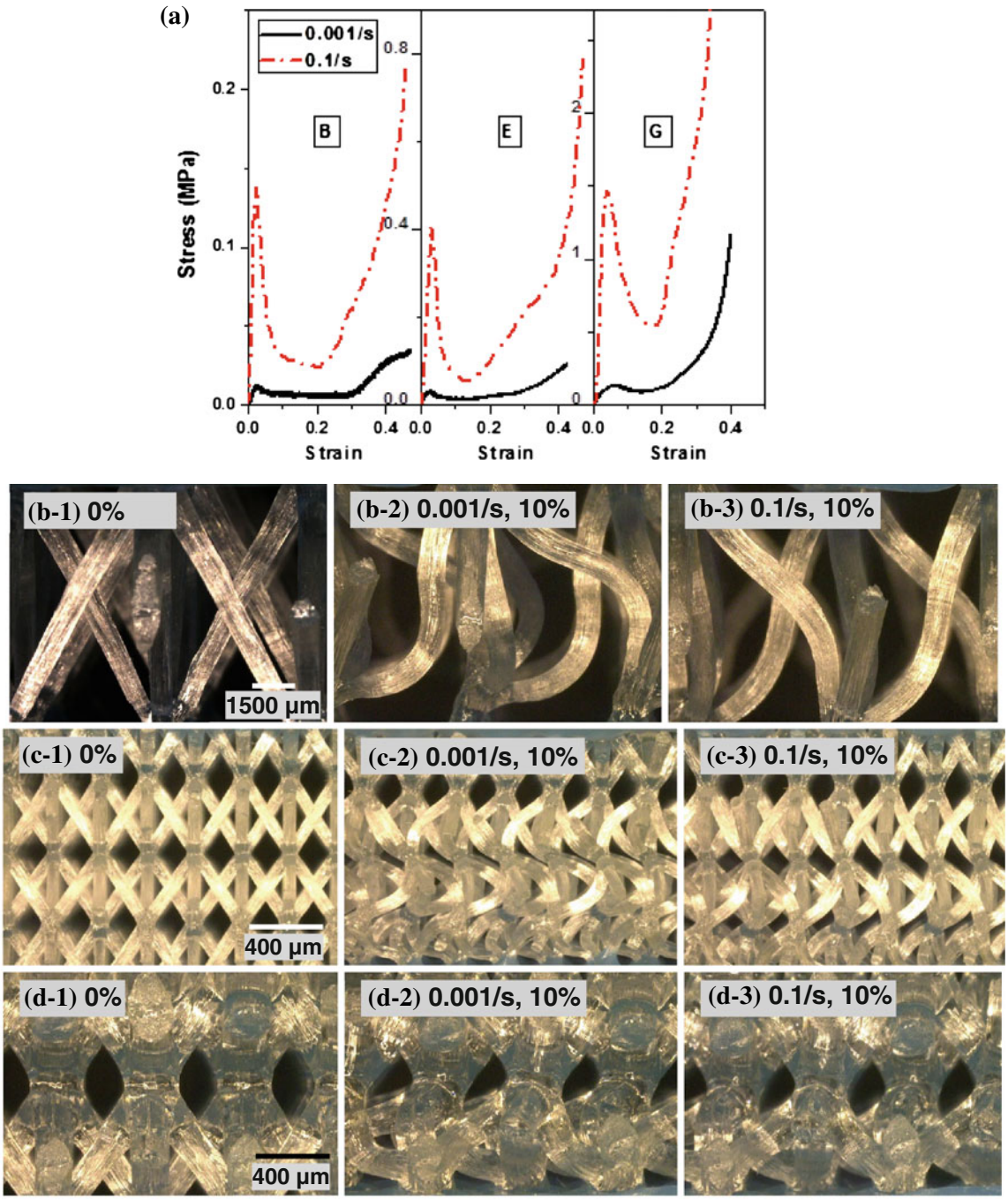

Fig. 4 **a** Representative responses of polymer micro-lattice sandwich structures in quasi-static compression; and the corresponding images of these structures at different strain rates as compressed to the strain of 10 %: **b** Specimen B; **c** Specimen E; **d** Specimen G

structures ranging from those with slender lattice members to those with stubby lattice members. The curves exhibit characteristics similar to those of composite lattice structures, including an approximately linear elastic region initially, reaching a peak stress followed by a stress drop associated with buckling of the lattice members, and finally a densification region [15]. Note that the structures can recover to the original shape even after 80 % compression strain. The failure mode for all structures tested at quasi-static rates was buckling, as shown in Figs. 4b–d. The buckling modes at different strain rates were different for structures with the same aspect ratio.

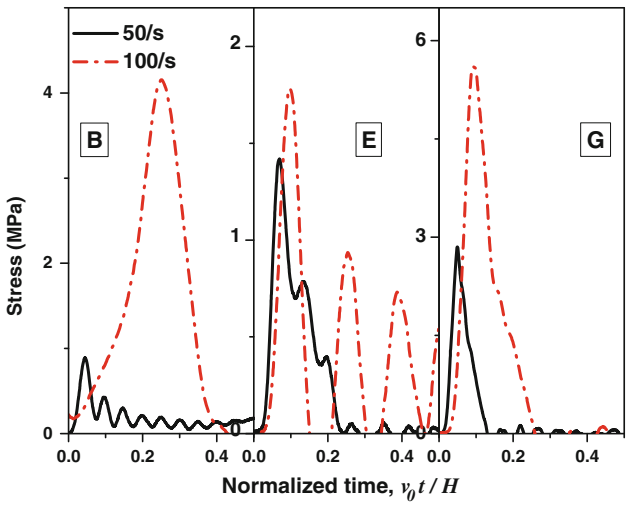

Fig. 5 Dynamic responses of polymer micro-lattice sandwich structures with different aspect ratios at strain rates 50 and 100/s

Dynamic compression

Dynamic compression tests were performed on the polymer micro-lattice specimens at strain rates 50 and 100/s, respectively. The corresponding dynamic responses are shown in Fig. 5. The stress was plotted against normalized time $v_0 t/H$, where v_0 is the impact velocity, t is the elapsed time for the instant of flat platen on the specimen and H is the height of the sandwich structures. The structures were also sensitive to strain rate in dynamic compression. The peak stress increased and the initial instability was delayed (see the normalized time at the peak stress) with increasing strain rate.

The two sequences of selected images, shown in Fig. 6 were recorded for Specimen B at strain rates of 50 and 100/s, respectively. The failure mode for Specimen B at a high strain rate was lattice member buckling. Comparing the image at a normalized time of 0.05 for a strain rate of 50/s with the image at a normalized time 0.25 for a strain rate of 100/s illustrates the postponed lattice member buckling associated with increased strain rate. The structures compressed at higher strain rate recovered their original shape almost completely after approximately half an hour. Figure 7a shows a recovered Specimen B after compression at 100/s. Meanwhile nodal rupture was also observed which should be attributed to high local strain.

Discussion

The strength of the micro-lattice sandwich structures is characterized using the normalized strength $\bar{\sigma}$, defined as $\bar{\sigma} = \sigma_{\mathrm{pk}}/\sigma_{0.001}$, where σ_{pk} is the peak stress measured at a given strain rate, and $\sigma_{0.001}$ is the compressive strength measured at a loading rate of 0.001/s. Figure 8a shows the dependence of strength on strain rate for structures with different aspect ratios. A non-linear peak stress increase is observed for structures of all aspect ratios, and the strength seems to be more sensitive at higher strain rate region. In particular, the structures with more slender lattice members (Specimens A and B) exhibit a strength increase of about 300 times at the strain rate of 0.001/s, while those with stubbier lattice members exhibit strength increases of $\sim$50 times (Specimen G), illustrating the strong dependence of strength on lattice slenderness ratio. Structures with slender lattice members are more sensitive than those with stubby lattice members at higher strain rates (observed transition starting from Specimen D with $d/l \approx 0.01$).

Because all the structures initially fail by buckling, the strength of polymer micro-lattice sandwich structures is given by $\sigma = \frac{k^2\pi^2 E_s}{4}\left(\frac{d}{l}\right)^2 \bar{\rho}\sin^2\theta$, where k is a constant that depends on the end constraint of the truss members, and E_s is the initial modulus of the parent polymer. Of the factors which contribute to structural strength enhancement mentioned by Xue and Hutchinson [27], strain-rate dependence of parent material is critical. Figure 8b shows the increase of modulus and strength for the parent polymer as a function of strain rate. The increase induced by strain rate sensitivity of the parent polymer can be expressed as $\sigma(\dot{\varepsilon}) = \frac{k^2\pi^2 E_s(\dot{\varepsilon})}{4}\left(\frac{d}{l}\right)^2 \bar{\rho}\sin^2\theta$, which linearly depends on the variation of $E_s(\dot{\varepsilon})$. The increase in modulus $E_s(\dot{\varepsilon})$ for the parent polymer is termed a material effect and included in Fig. 8a. The comparisons in Fig. 8a between the strength increase of the structures and the modulus increase of parent polymer indicates the additional inertial effect on the strength of micro-lattice core. The micro-inertial effect is apparent at high strain rates, particularly for structures with slender trusses ($d/l < 0.01$). Moreover, the delayed onset of truss buckling with increasing strain rate, illustrated in Figs. 4, 6, also provides additional evidence of the inertial stabilization effect.

The governing failure mode of specimen B is Euler buckling, which occurs when peak stress is achieved. However, node rupture was also observed after compression at 100/s which demonstrated the high localized strain at the node, as shown in Fig. 7. The macroscopic failure mode transition for a specific structure, truss buckling or fracture, will depend on the strength-to-modulus ratio σ_s/E_s of the polymer materials in quasi-static loading [14], although the materials effect $\sigma_s(\dot{\varepsilon})/E_s(\dot{\varepsilon})$ is only one factor involved in a high strain rate application.

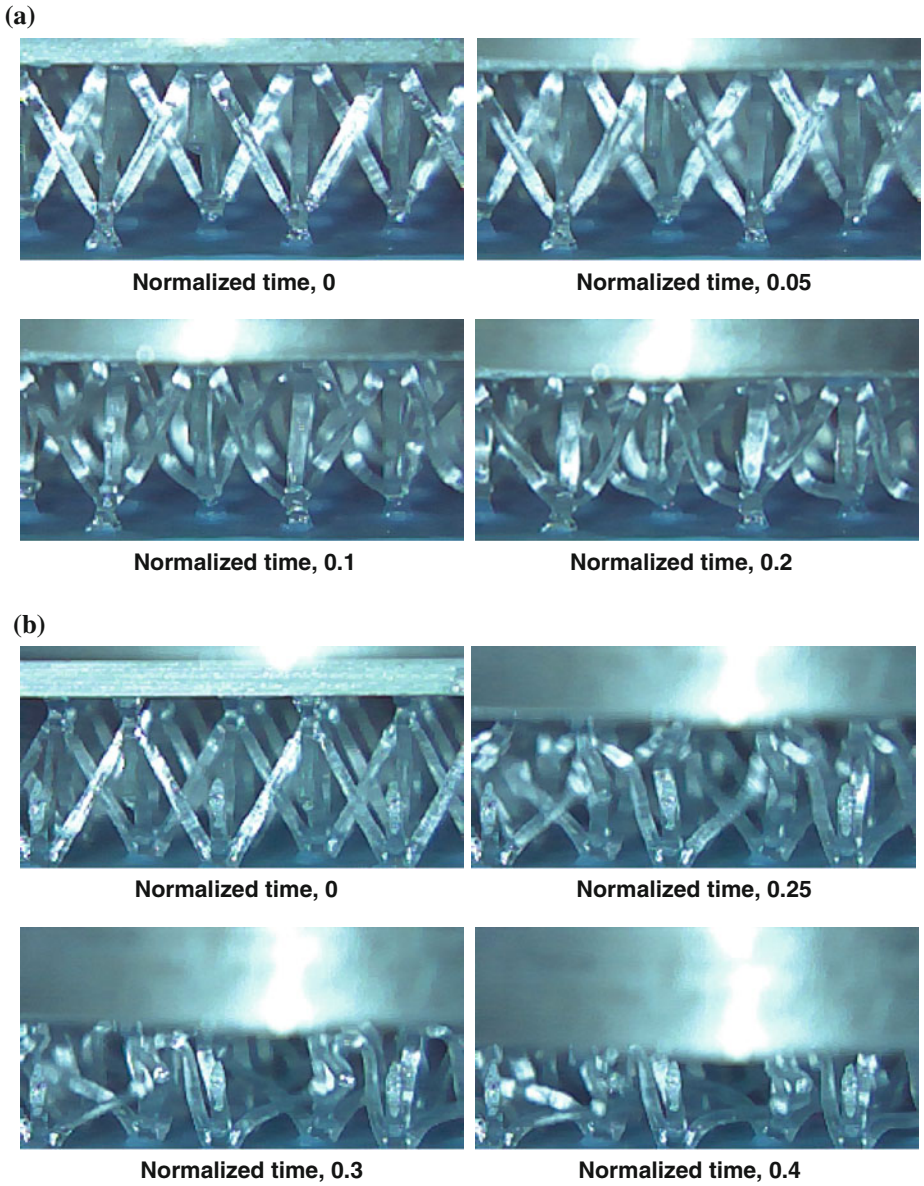

Fig. 6 High-speed images for Specimen B compressed at **a** 50/s and **b** 100/s

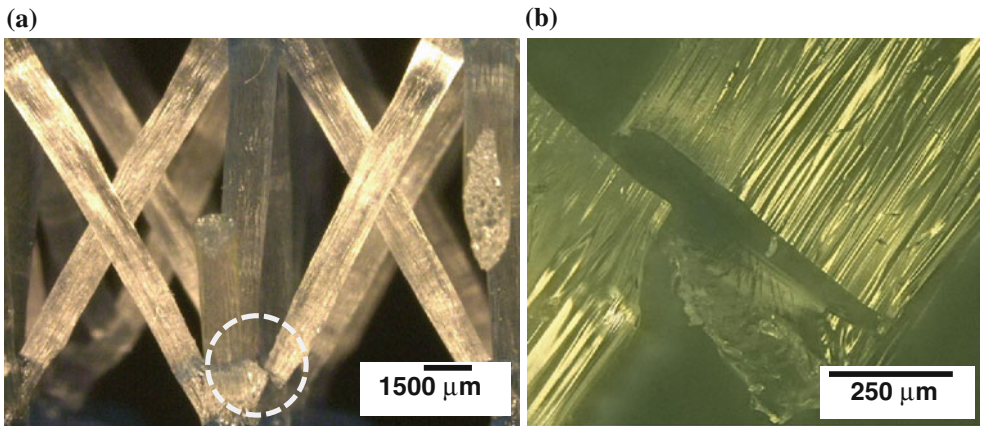

Fig. 7 **a** Optical image of recovered Specimen B after dynamic compression at 100/s; **b** nodal rupture at one truss end marked in (**a**)

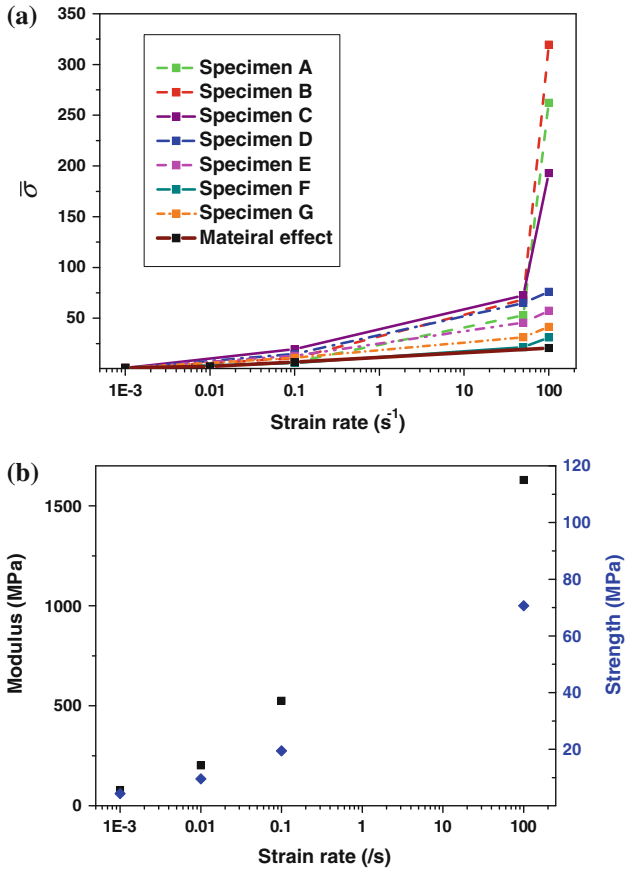

Fig. 8 **a** Strength enhancement as a function of strain rate for polymer micro-lattice structures with different aspect ratio *d*/*l*; **b** compressive modulus (*squares*) and strength (*diamonds*) of parent polymer as a function of strain rate. The modulus increase of polymer recognized as material effect on strength enhancement of the structure is also included in (**a**)

Conclusions

Flexible micro-lattices were produced using an interconnected pattern of self-propagating polymer waveguides [18]. The strain-rate sensitivity and inertial stabilization of the micro-lattice structures was determined by measurements. Seven groups of micro-lattice sandwich structures with different lattice geometries were compressed at different strain rates, and all structures recovered nearly to their original shape for all strain rates. The structural strength increased with strain rate. Inertial stabilization effects were decoupled from materials strain-rate effect, while both contributed to the observed strength increase. The micro-inertial effects were more pronounced in micro-lattice structures with greater aspect ratio (correspond to $d/l < 0.01$), particularly at high strain rates (>1/s).

The T_g of the parent polymer was below room temperature and shifted by $\sim$6.6 °C per decade of strain rate. Accordingly, the structures exhibited behavior translating from rubbery state to leathery state with elevated strain rate. The material characteristics together with structural inertial effects show implications in the design of micro-lattice materials that are compliant and energy absorbing at low strain rates but become stronger and impact resistant at high strain rates. These results are relevant for a range of strain-rate dependent applications, including crashworthy vehicles and blast resistant structures.

Acknowledgements S. Nutt acknowledges support from the Mc. Gill Composites Center. L.Z. Wu would like to thank the Major State Basic Research Development Program of China (973 Program, No. 2011CB610303). S. Yin gratefully acknowledges the support from China Scholarship Council (CSC) during the visit at University of Southern California.

References

1. Evans AG, Hutchinson JW, Fleck NA, Ashby MF, Wadley HNG (2001) Prog Mater Sci 46(3–4):309
2. Wang J, Evans AG, Dharmasena K, Wadley HNG (2003) Int J Solids Struct 40(25):6981
3. Chiras S, Mumm DR, Evans AG, Wicks N, Hutchinson JW, Dharmasena K, Wadley HNG, Fichter S (2002) Int J Solids Struct 39(15):4093
4. Rathbun HJ, Wei Z, He MY, Zok FW, Evans AG, Sypeck DJ, Wadley HNG (2004) J Appl Mech 71(3):368
5. Kooistra GW, Deshpande VS, Wadley HNG (2004) Acta Mater 52(14):4229
6. Queheillalt DT, Wadley HNG (2005) Mater Sci Eng A 397(1–2):132
7. Bele E, Bouwhuis BA, Hibbard GD (2008) Mater Sci Eng A 489(1–2):29
8. Wadley HNG (2006) Philos Trans R Soc A 364(1838):31
9. Wadley HNG (2002) Adv Eng Mater 4(10):726
10. Wadley HNG, Fleck NA, Evans AG (2003) Compos Sci Technol 63(16):2331
11. Steeves CA, He MY, Kasen SD, Valdevit L, Wadley HNG, Evans AG (2009) J Appl Mech 76(3):9
12. Valdevit L, Vermaak N, Zok FW, Evans AG (2008) J Appl Mech 75(6):061022
13. Bouwhuis B, Bele E, Hibbard G (2008) J Mater Sci 43(9):3267. doi:10.1007/s10853-008-2529-x
14. Yin S, Wu L, Ma L, Nutt S (2012) Composites Part B 43(4):1749
15. Yin S, Wu L, Ma L, Nutt S (2011) Compos Struct 93(12):3104
16. Sharp DN, Campbell M, Dedman ER, Harrison MT, Denning RG, Turberfield AJ (2002) Opt Quantum Electron 34(1–3):3
17. Haske W, Chen VW, Hales JM, Dong W, Barlow S, Marder SR, Perry JW (2007) Opt Express 15(6):3426
18. Jacobsen AJ, Barvosa-Carter W, Nutt S (2007) Adv Mater 19(22):3892
19. Jacobsen AJ, Barvosa-Carter W, Nutt S (2007) Acta Mater 55(20):6724
20. Jacobsen AJ, Barvosa-Carter W, Nutt S (2008) Acta Mater 56(6):1209
21. Sarva SS, Deschanel S, Boyce MC, Chen W (2007) Polymer 48(8):2208
22. Yi J, Boyce MC, Lee GF, Balizer E (2006) Polymer 47(1):319
23. McShane GJ, Stewart C, Aronson MT, Wadley HNG, Fleck NA, Deshpande VS (2008) Int J Solids Struct 45(16):4407
24. Park S, Russell BP, Deshpande VS, Fleck NA (2012) Composites Part A 43(3):527

25. Song B, Chen WW, Dou S, Winfree NA, Kang JH (2005) Int J Impact Eng 31(5):509
26. Kazemahvazi S, Russell BP, Zenkert D (2012) Compos Struct 94(11):3300
27. Xue Z, Hutchinson JW (2006) Int J Numer Methods Eng 65(13):2221
28. Vaziri A, Xue ZY (2007) J Mech Mater Struct 2(9):1743
29. Vaziri A, Xue ZY, Hutchinson JW (2007) J Mech Mater Struct 2(10):1947
30. Hou B, Zhao H, Pattofatto S, Liu JG, Li YL (2012) Int J Solids Struct 49(19–20):2754
31. Tang X, Prakash V, Lewandowski JJ, Koolstra GW, Wadley HNG (2007) Acta Mater 55(8):2829